Electronic Supplementary Information (ESI)

Phase Diagram Exploration of Tc-Al-B: from Bulk Tc_2AlB_2 to Two-dimensional Tc_2B_2

Heng Zhang,[ab] Junjie Wang,*[a] Mohammad Khazaei,[c] Frédéric Guegan,[b] Gilles Frapper*[ba]

[a] State Key Laboratory of Solidification Processing and International Centre for Materials Discovery, School of Materials Science and Engineering, Northwestern Polytechnical University, Xi'an, Shaanxi 710072, People's Republic of China

[b] Applied Quantum Chemistry group, E4, IC2MP, UMR 7285 Poitiers university-CNRS, 4 rue Michel Brunet TSA 51106 - 86073 Poitiers Cedex 9, France

[c] Department of Physics, University of Tehran, North Karegar Ave., Tehran, Iran

*Corresponding authors: wang.junjie@nwpu.edu.cn, gilles.frapper@univ-poitiers.fr

Contents

S1. Methodology

S1.1 Evolutionary algorithm (USPEX)

USPEX (Universal Structure Predictor: Evolutionary Xtallography) is a global evolutionary search algorithm for structure prediction developed by the A.R. Oganov laboratory since 2004 (see http://uspex-team.org/en/uspex/overview).[1-3] In this work, this evolutionary algorithm EA code is interfaced with VASP (Vienna *Ab initio* Simulation Package) for DFT structure relaxation (shape, volume, atomic positions are optimized by VASP).[4] The EA development allows the prediction of the stable and metastable structures knowing only the chemical composition at zero Kelvin. Simultaneous searches for stable compositions and structures are also possible. This variable-composition technique is used to investigate stable compounds in the Tc-Al-B ternary phase diagram at the ambient condition, at zero Kelvin. For the resulting bulk $Tc_xAl_yB_z$ (where x, y, z are positive integers) minimum, a fixed composition is then employed to locate the most stable structure. The latter EA search is performed at least twice to ensure convergence to a global minimum.

A large number (150) of randomly created structures is chosen in the first generation of the EA. In the next generations, 100 structures are generated. What is the generation process? For each parent structure from a previous generation, the fitness is computed as the free enthalpy derived from an ab initio total energy calculation (here VASP). All structures are then tested against three constraints: interatomic distances, cell angles and cell lengths. 80% of the best (i.e., lowest enthalpy) optimized structures are selected to participate in producing the next generation. A new candidate structure is produced from parent structures using one of four operators defined in Refs 1-3: (i) heredity, (ii) permutation, (iii) lattice mutations, and (iv) atomic mutation, which account for 50, 10, 10, and 10% of the structures in the new generation. The remaining 20% are randomly generated (similarly to those of the first generation). A fixed composition EA search is considered achieved when the same global structure minimum is found during 10 consecutive generations. Typically, such search requires between 10 and 30 generations.

S1.2 DFT calculations (VASP)

First-principles calculations are performed using the projected-augmented-wave (PAW) method as implemented in VASP (version 5.4.4).[5] Exchange-correlation energy is treated using Perdew-Burke-Ernzerhof (PBE) within the generalized gradient approximation (GGA)[6,7] A kinetic cutoff energy of 520 eV is used for the wavefunction expansion with a Monkhorst-Pack k mesh grid with a spacing of $2\pi \times 0.04$ Å^{-1}. This ensure that enthalpy converges to a criterion lower than 1×10^{-5} eV per cell. In USPEX calculation, 5 successive steps of increasing convergence accuracy are usually required (i.e., 5 INCAR files). An illustration of this local optimization procedure is given in the PhD manuscript of B. Huang, "Computational materials discovery: prediction of carbon dioxide and nitrogen-based compounds under pressure using density functional theory and evolutionary algorithm", supervised by Pr. G. Frapper, IC2MP, Poitiers University (France), Dec. 2017 http://theses.univ-poitiers.fr/notice/view/59262). The parameters and criterion associated with VASP calculations then correspond to the last (5th) step of the highest accuracy.

Ab initio molecular dynamics (AIMD) simulations based on DFT are also carried out using VASP code to examine the thermal stability of (meta)stable candidate phases. AIMD calculations were performed up to 1000 K with the canonical (NVT) ensemble.[8] The timestep was 2 fs, and the total simulation time was as long as 12 ps. In such AIMD simulations, the 2×2×2 supercells are employed for bulk $Tc_xAl_yB_z$, 4×4 supercells for 2D Tc_2B_2 and its derivatives, and the Brillouin zone integration is restricted to the Γ point of the supercell.

S1.3 Phonon calculations and force constants

In this work, first principles phonon calculations with a finite displacement method at quasi-harmonic level were done using the open-source package PHONOPY (https://atztogo.github.io/phonopy/).[9] Supercell structures with (or without) displacements are created from a unit cell fully considering crystal symmetry. In general, a 2×2×2 supercell is needed, sometimes higher. Force constants are calculated using the structure files POSCAR (VASP code). In addition, the effect of zero-point energy (ZPE) on the stability of bulk $Tc_xAl_yB_z$ compounds was studied. We find that the inclusion of ZPE only moderately shift the stability Fig.s but does not change

the phase stability order. Thus, the energies presented in this manuscript are not ZPE corrected.

To evaluate the strength of the bonds, the force constants are computed to be the second derivative of the total energy with respect to finite displacements of atoms i and j along the *x*, *y*, and *z* directions.[10,11] It is a 3 × 3 matrix as the output during the phonon calculations. Since the trace of the force constant matrix is independent of the coordinate system, i.e., invariant under a coordinate rotation, we consider the value of the trace of the force constant matrix and refer to this scalar quantity as the force constant F_{ij} between atoms i and j.[12,13]

S1.4 Mulliken population

Mulliken charges and bond populations are calculated based on the formalism described by Segall et al.[13,14] Population analysis in CASTEP is computed using a projection of the PW states onto a localized basis using a technique described by Sanchez-Portal et al.[15] Population analysis of the resulting projected states is then performed using the Mulliken formalism.[16] This technique is widely used in the analysis of electronic structure calculations performed with LCAO basis sets.

S1.5 Bader charge analysis

When we performed Bader charge analysis in VASP, the reference charge density we chose was the sum of the core charge (AECCAR0) and valance charge (AECCAR2). (http://theory.cm.utexas.edu/henkelman/code/bader/). The valance electron configurations in our VASP calculations are Tc($5s^2 4d^5$), Al($3s^2 3p^1$), B($2s^2 2p^1$), O($2s^2 2p^4$), H($1s^1$), F($2s^2 2p^5$).

S1.6 Mechanical properties

A necessary condition for the thermodynamic stability of a crystal lattice is that the crystal should be mechanically stable with respect to arbitrary (small) homogeneous deformations. Elastic stability criteria for bulk cubic crystals and more different crystal classes were well understood in the work of Born, et al.[17-19] In VASP, IBRION=6 and ISIF≥3 tags allow to calculate the elastic constants. The elastic tensor is determined by performing six finite distortions of the lattice and deriving the elastic constants from the strain-stress relationship.[20]

The stiffness matrix for an orthorhombic crystal has nine independent constants (C_{11}, C_{12}, C_{13}, C_{22}, C_{23}, C_{33}, C_{44}, C_{55}, C_{66}) and no relationships between them. The necessary and sufficient Born criteria for an orthorhombic system:

$C_{11} > 0$, $C_{11}C_{22} > C_{12}C_{12}$,

$C_{11}C_{22}C_{33} + 2C_{12}C_{13}C_{23} - C_{11}C_{23}C_{23} - C_{22}C_{13}C_{13} - C_{33}C_{12}C_{12} > 0$,

$C_{44} > 0$, $C_{55} > 0$, $C_{66} > 0$.

Monoclinic and triclinic crystal systems have 13 and 21 independent elastic constants, respectively. The necessary and sufficient Born criteria for monoclinic and triclinic systems:

K3=det$|C_{ij}|$, i,j $\leq$ 6, K3 >0.

The elastic matrix of 2D materials was decreased into 3×3 and six elastic constants are C_{11}, C_{12}, C_{22}, C_{16}, C_{26} and C_{66} using the standard Voigt notation:1-*xx*, 2-*yy*, 6-*xy*. In 2D rectangular unit-cells, C_{16} and C_{26} are zero. The calculated elastic constants C_{11}, C_{12}, C_{22} and C_{66} in 2D rectangular materials should satisfy necessary mechanical equilibrium conditions for mechanical stability: $C_{11}C_{22}$-$C_{12}C_{21}$>0 and C_{11}, C_{22}, C_{66}>0.[21]

In terms of these elastic constants, the 2D Young's moduli (in-plane stiffness) for the stain in the [10] and [01] direction are,[22]

$Y_{2D\text{-}x} = (C_{11}C_{22}\text{-}C_{12}C_{12})/C_{22}$, and $Y_{2D\text{-}y} = (C_{11}C_{22}\text{-}C_{12}C_{12})/C_{11}$.

The corresponding Poisson's ratio are,

$v_{2D\text{-}xy} = C_{12}/C_{22}$, and $v_{2D\text{-}yx} = C_{12}/C_{11}$.

The 2D shear modulus is $G_{2D} = C_{66}$.

S1.7 Bonding energy and separation energy ratio

In layered ternary MAB and Tc-B-Al phases, the bonding energy can be calculated by from the energy difference of two configurations (see Fig. S1): (a) a slab in vacuum (~35 Å) consisting of thick atomic layers (~40 Å) and (b) the specific layer of the slab being separated with the interlayer distance of ~17 Å. The separation energy ratio σ is calculated as bonding energy ratios at M/Al and M/B interfaces. The atomic positions in both configurations were relaxed in the fixed lattice.[23,24]

S1.8 Adsorption energy

To ascertain the adsorption thermodynamically stability between the ligands (L=H, F, O, OH) and 2D Tc_2B_2, the absorption energy is calculated by the formula,[25]

E_{ad}=E(Tc_2B_2-L_n)-E(Tc_2B_2)-nE(L),

E(TcB-L_n), E(Tc_2B_2), and E(L) are the energy of ligands on the 2D Tc_2B_2 3×3 supercell, pristine 2D Tc_2B_2, and atomic energy in H_2, F_2, O_2, or O_2+H_2 gas state. And n is the number of ligands on 2D Tc_2B_2 3×3 supercell and for the case of the full coverage of the ligands, n reaches the maximum of 18.

S2. Stable bulk binary Al-B, Tc-Al and ternary phases

S2.1 Thermodynamical stability of bulk Al-B and Tc-Al phase

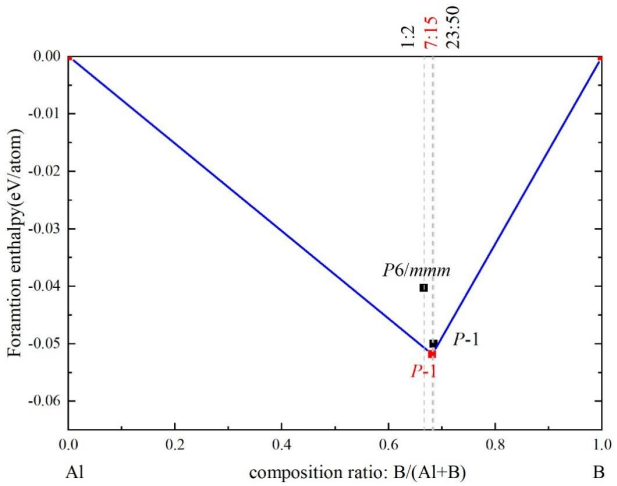

Fig. S1 Energy convex hull of binary Al-B system at ambient condition. The stable phase (*P*-1 Al_7B_{15}) on the convex hull line (blue) is indicated in red square.

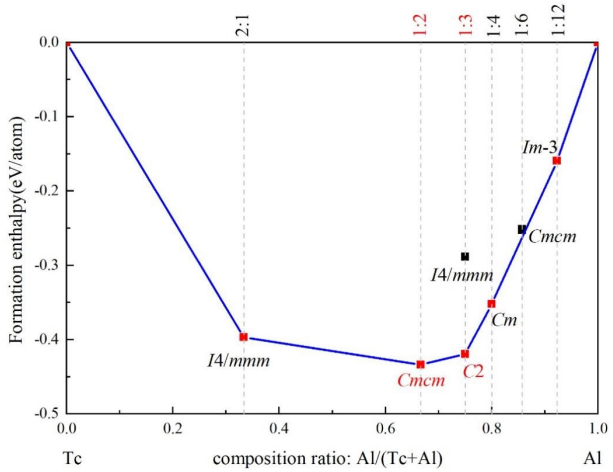

Fig. S2 Energy convex hull of binary Tc-Al system at ambient condition. Two new compositions (1:2 *Cmcm*, 1:3 *C*2) are indicated in red.

S2.2 Dynamical stability

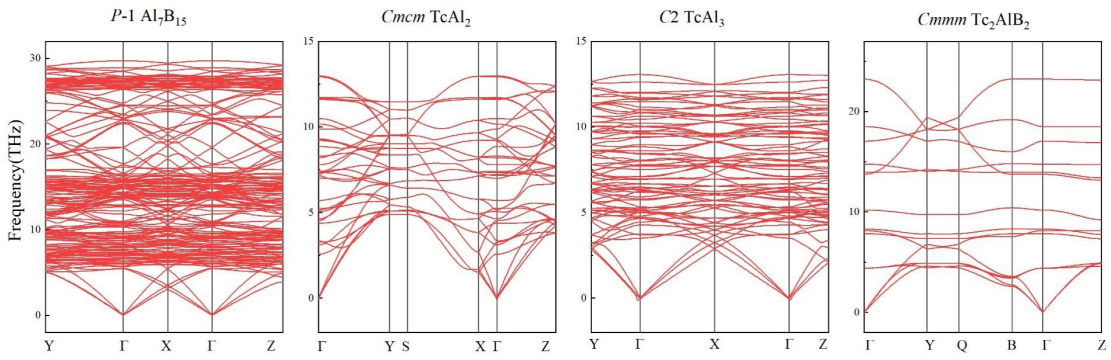

Fig. S3 Phonon dispersion curves of bulk *P*-1 Al_7B_{15}, *Cmcm* $TcAl_2$, *C*2 $TcAl_3$ and *Cmmm* Tc_2AlB_2.

S2.3 Thermal (kinetic) stability

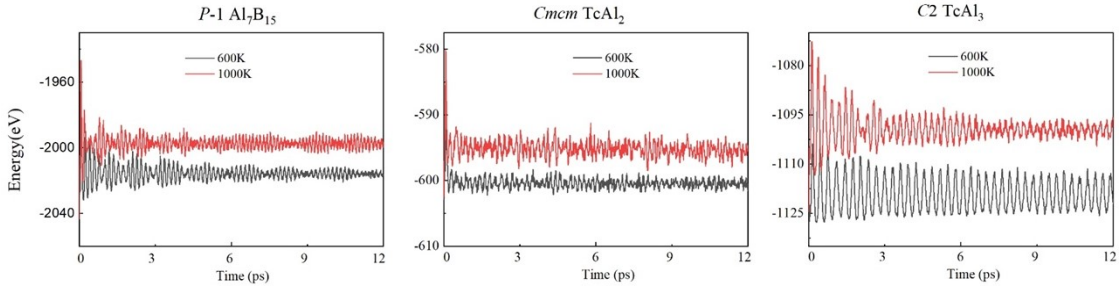

Fig. S4 Energy fluctuations of bulk *P*-1 Al_7B_{15}, *Cmcm* $TcAl_2$, and *C*2 $TcAl_3$ during AIMD simulations at specific temperatures, T = 600K, 1000K.

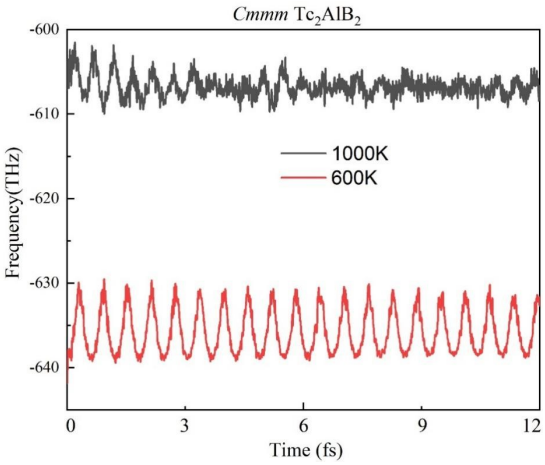

Fig. S5 Energy fluctuations of bulk *Cmmm* Tc_2AlB_2 during the AIMD simulations at specific temperatures, T = 600K, 1000K.

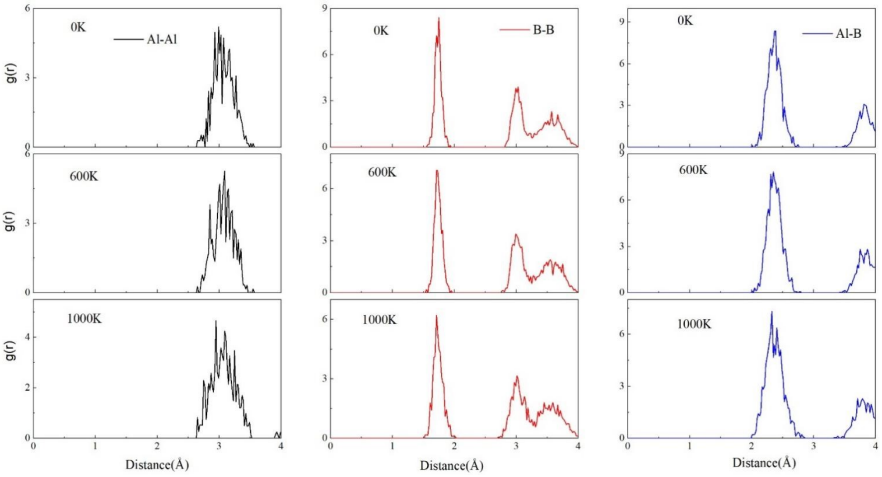

Fig. S6 Radial distribution functions (RDF) for the Al-Al, B-B and Al-B contacts during AIMD simulations in bulk *P*-1 Al_7B_{15} at T = 0 K, 600 K, 1000 K

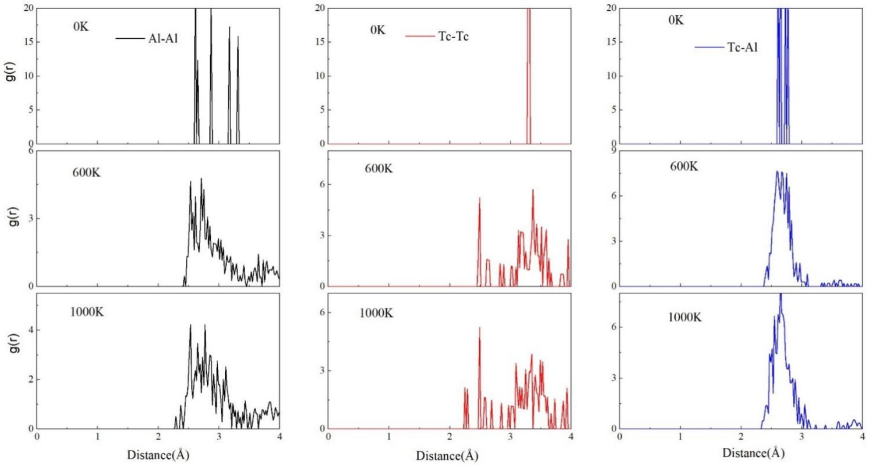

Fig. S7 Radial distribution functions (RDF) for the Al-Al, Tc-Tc, Tc-Al contacts during AIMD simulations in bulk *Cmcm* $TcAl_2$ at T = 0 K, 600 K, 1000 K.

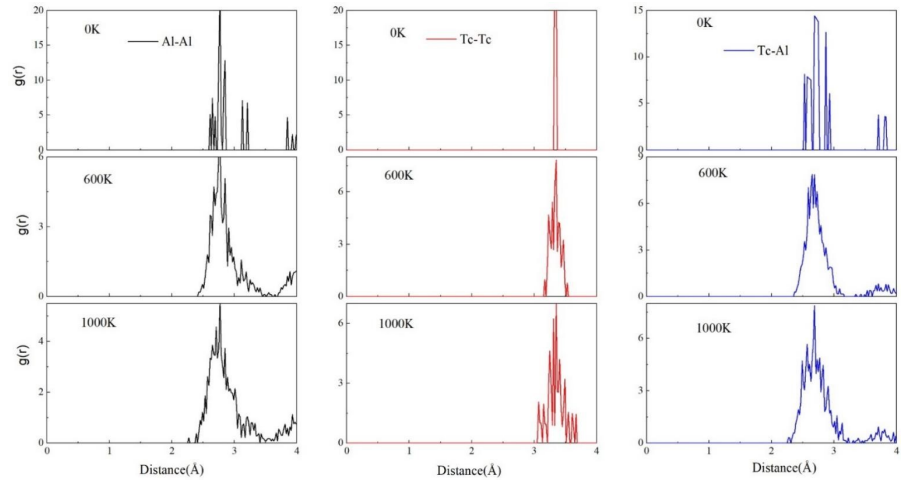

Fig. S8 Radial distribution functions (RDF) for the Al-Al, Tc-Tc, Tc-Al contacts during AIMD simulations in bulk *C*2 $TcAl_3$ at T = 0 K, 600 K, 1000 K.

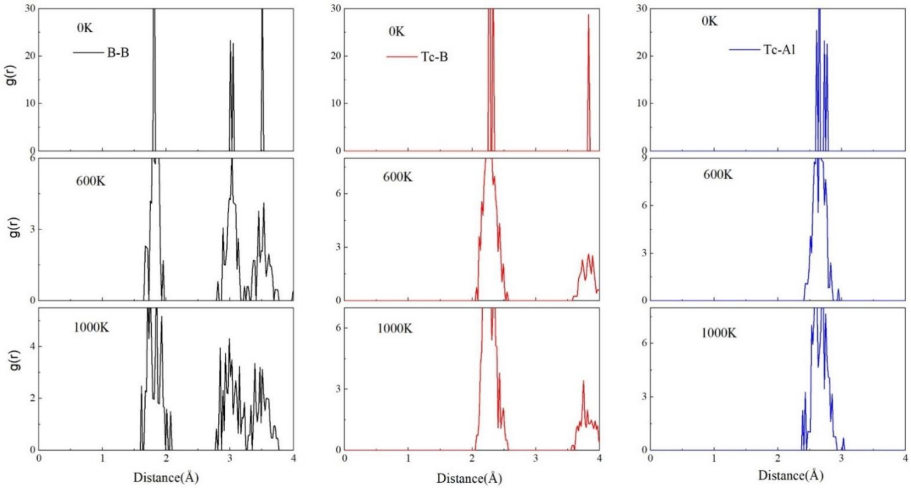

Fig. S9 Radial distribution functions (RDF) for the B-B, Tc-B, and Tc-Al contacts in bulk *Cmmm* Tc_2AlB_2 during AIMD simulations at T = 0 K, 600 K, 1000 K.

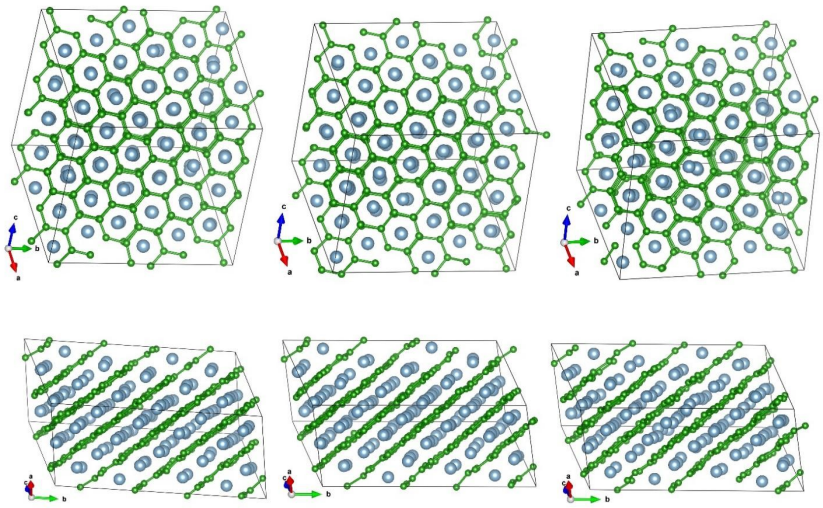

0K 600K 1000K

Fig. S10 Snapshots of the bulk *P*-1 Al_7B_{15} supercell (2×2×2) at ambient pressure at the end of 12 ps, T =0K, 600K, 1000K.

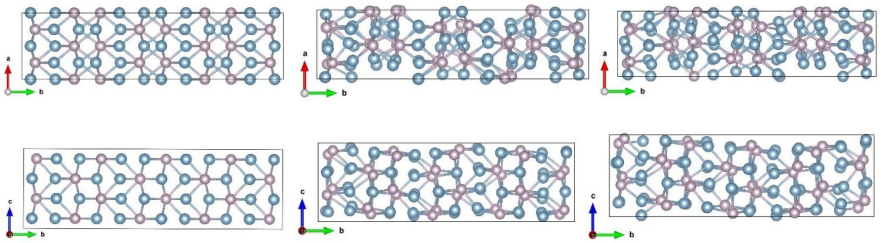

0K 600K 1000K

Fig. S11 Snapshots of the bulk *Cmcm* $TcAl_2$ supercell (2×2×2) at ambient pressure at the end of 12 ps, T =0K, 600K, 1000K.

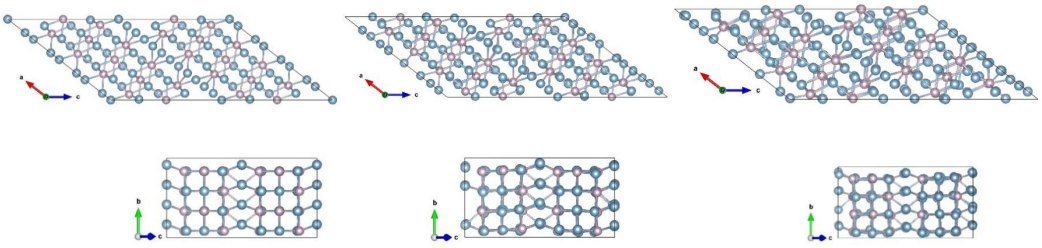

0K 600K 1000K

Fig. S12 Snapshots of the bulk *C*2 $TcAl_3$ supercell (2×2×2) at ambient pressure at the end of 12 ps, T =0K, 600K, 1000K

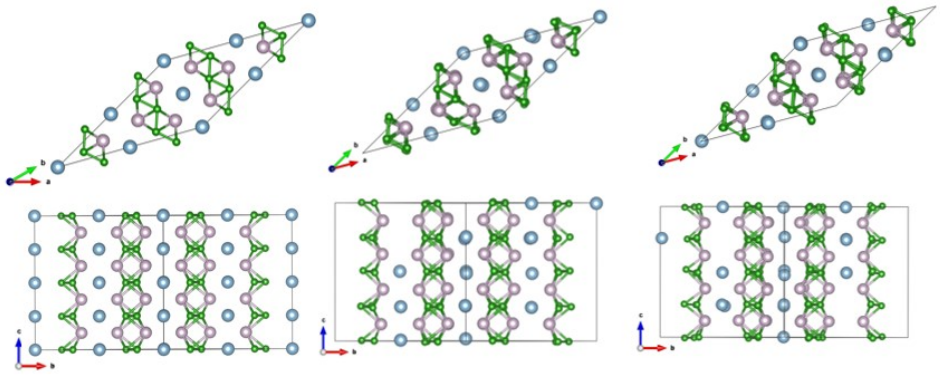

0K 600K 900K

Fig. S13 Snapshots of the bulk *Cmmm* Tc_2AlB_2 supercell (2×2×2) at ambient pressure at the end of 12 ps.

S2.4 Electronic band structure and DOS

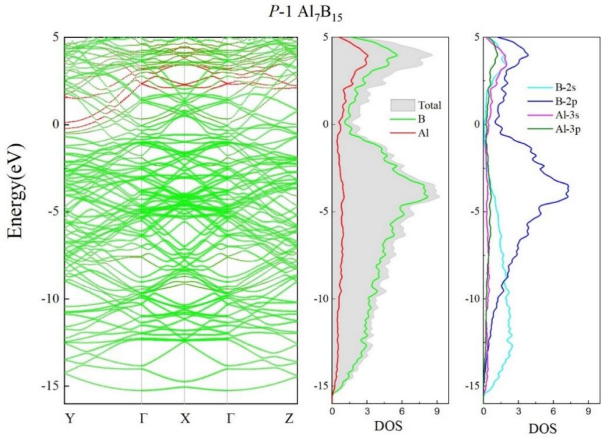

Fig. S14 Projected band structure and DOS of bulk *P*-1 Al_7B_{15} phase. The Fermi energy is set to zero.

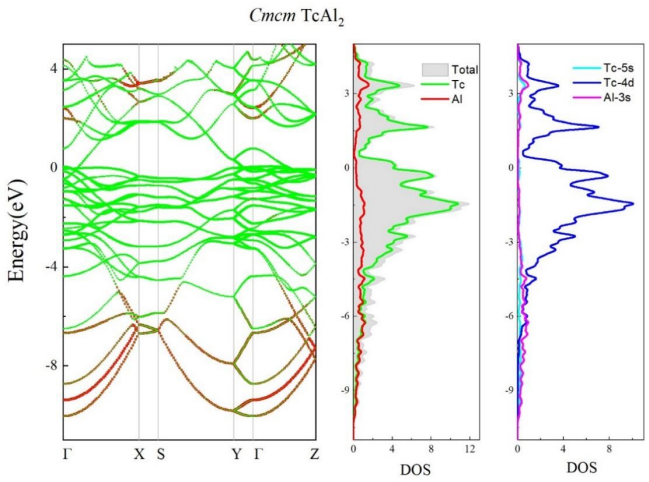

Fig. S15 Projected band structure and DOS of bulk *Cmcm* $TcAl_2$ phase. The Fermi energy is set to zero.

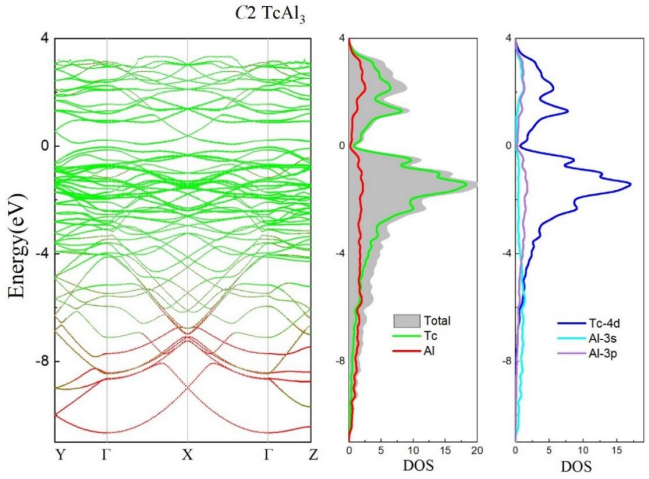

Fig. S16 Projected band structure and DOS of bulk *C*2 $TcAl_3$ phase. The Fermi energy is set to zero.

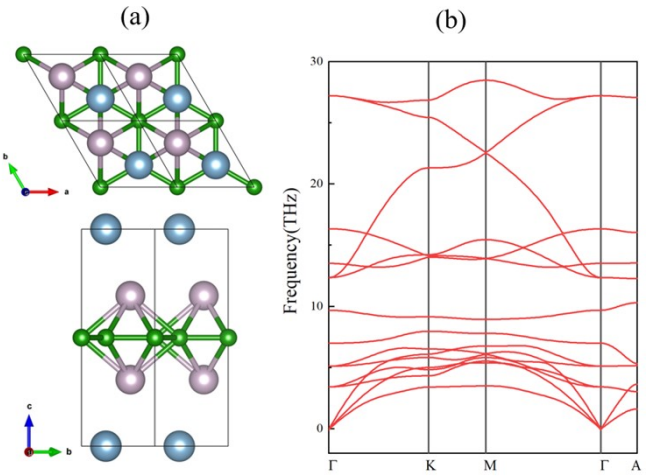

Fig. S17 Hexagonal *P*-6*m*2 Tc_2AlB_2: (a) top and side view of structure motif; (b) calculated phonon bandstructure.

S3 Metastable ternary Tc-Al-B compounds

S3.1 Structure configuration of metastable Tc-Al-B compounds

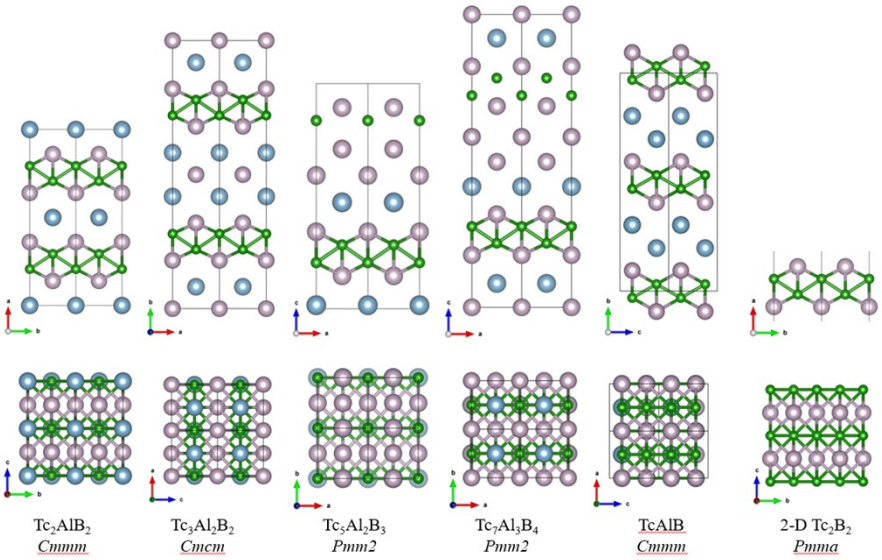

Fig. S18. Family of bulk (meta)stable $Tc_xAl_yB_z$ compounds, *Cmmm* Tc_2AlB_2, *Cmmm* $Tc_3Al_2B_2$, *Pmm*2 $Tc_5Al_2B_3$, *Pmm*2 $Tc_7Al_3B_4$, and *Cmcm* $TcAlB_2$ in which 2D Tc_2B_2 blocks present infinite zigzag boron chains.

S3.2 Dynamical stability

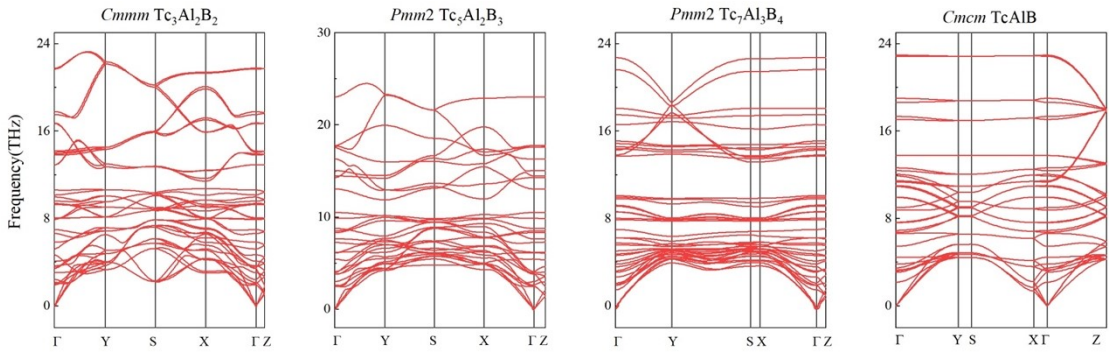

Fig. S19 Phonon dispersion curves of metastable bulk $Tc_xAl_yB_z$ compounds, *Cmmm* $Tc_3Al_2B_2$, *Pmm*2 $Tc_5Al_2B_3$, *Pmm*2 $Tc_7Al_3B_4$, and *Cmcm* TcAlB.

S3.3 Thermal stability

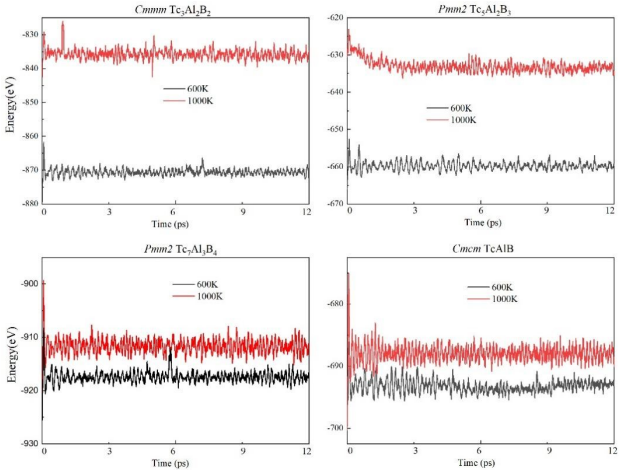

Fig. S20 Energy fluctuation of metastable bulk $Tc_xAl_yB_z$ compounds during AIMD simulations at specific temperatures, T = 600K, 1000K.

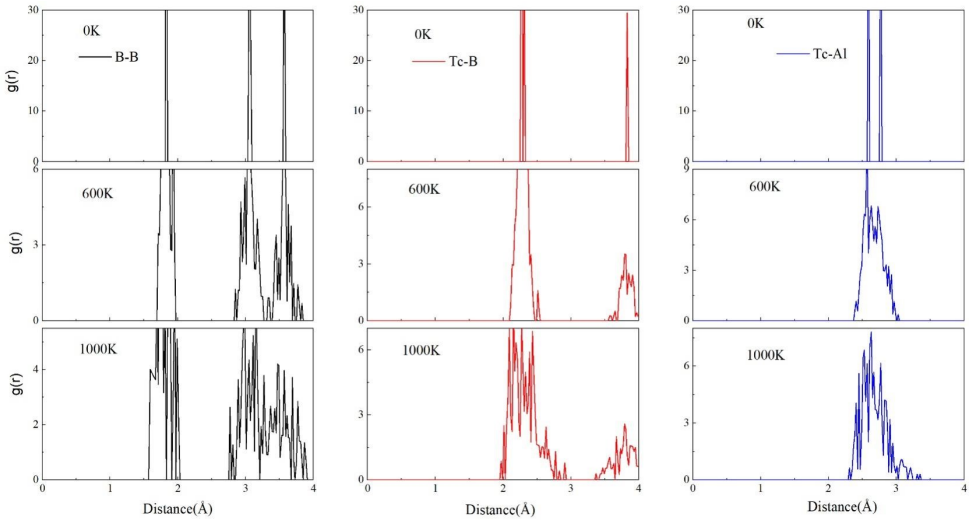

Fig. S21 Radial distribution functions (RDF) for the B-B, Tc-B, Tc-Al contacts in *Cmmm* $Tc_3Al_2B_2$ during AIMD simulations at T = 0 K, 600 K, 1000 K.

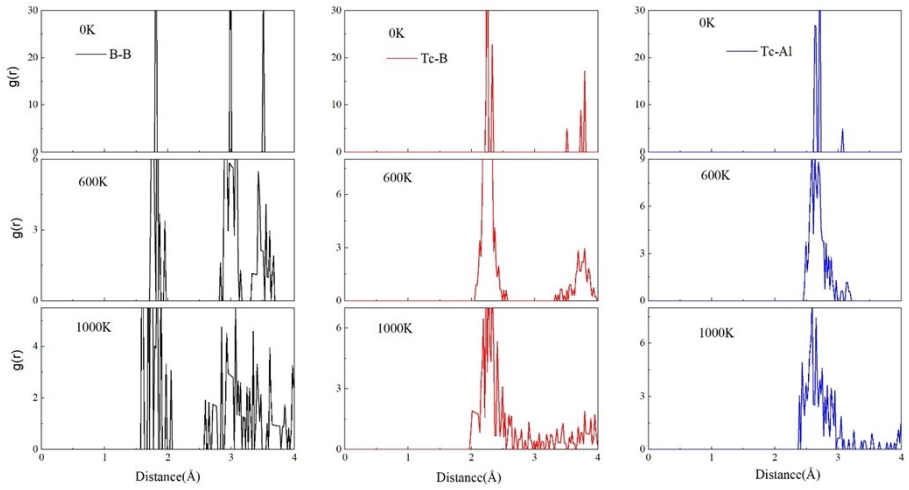

Fig. S22 Radial distribution functions (RDF) for the B-B, Tc-B, Tc-Al contacts in *Pmm*2 $Tc_5Al_2B_3$ during AIMD simulations at T = 0 K, 600 K, 1000 K.

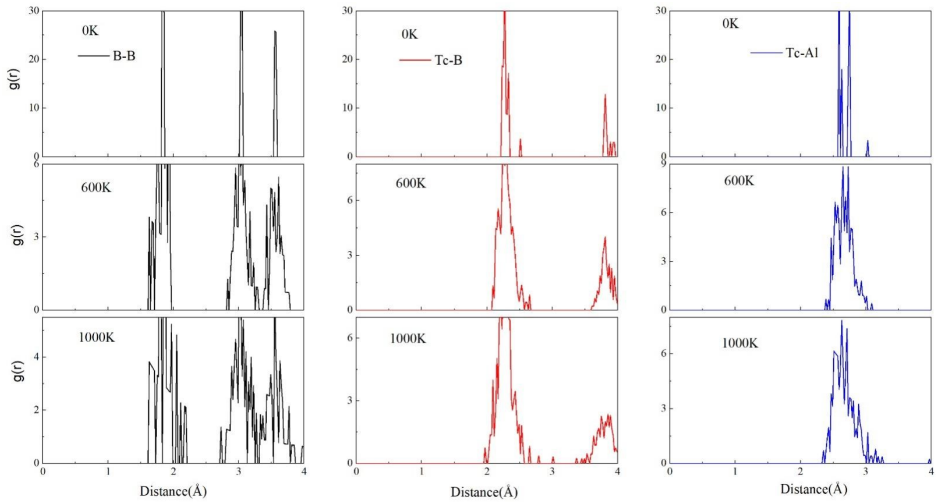

Fig. S23 Radial distribution functions (RDF) for the B-B, Tc-B, Tc-Al contacts in *Pmm*2 $Tc_7Al_3B_4$ during AIMD simulations at T = 0 K, 600 K, 1000 K.

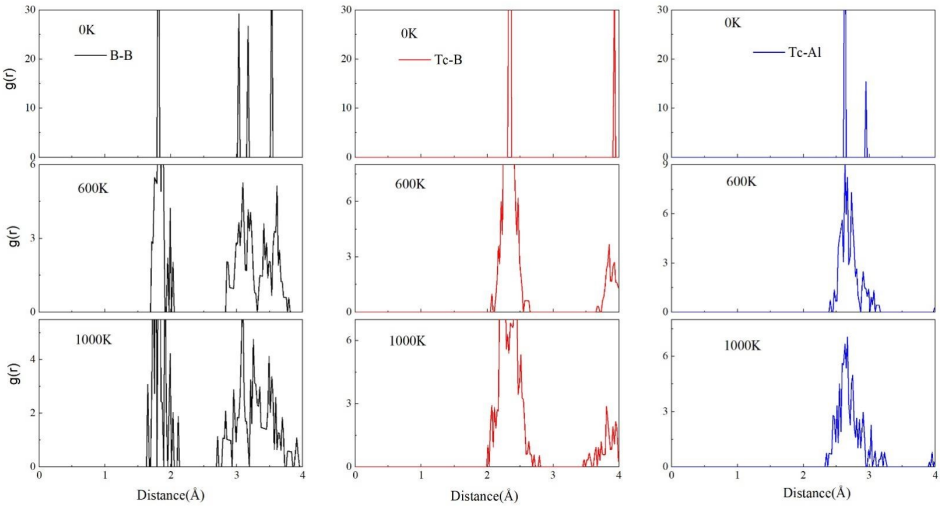

Fig. S24 Radial distribution functions (RDF) for the B-B, Tc-B, Al-B, Tc-Al contacts in *Cmcm* TcAlB during AIMD simulations at T = 0 K, 600 K, 1000 K.

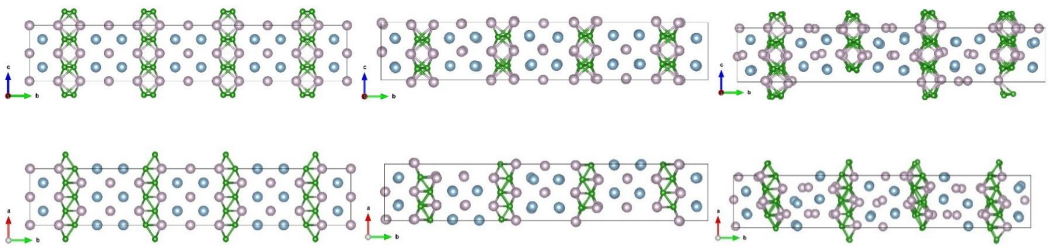

0K 600K 1000K

Fig. S25 Snapshots of *Cmmm* $Tc_3Al_2B_2$ supercell (2×2×2) at ambient pressure at the end of 12 ps, at T = 0 K, 600 K, 1000 K

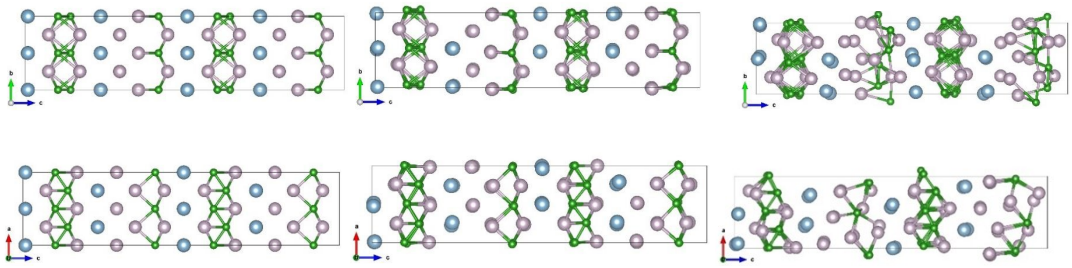

0K 600K 1000K

Fig. S26 Snapshots of *Pmm*2 $Tc_5Al_2B_3$ supercell (2×2×2) at ambient pressure at the end of 12 ps.

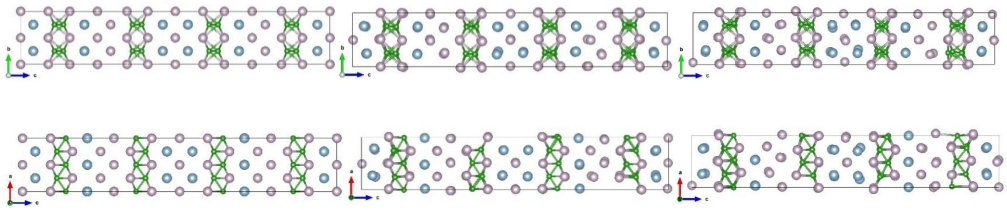

0K 600K 1000K

Fig. S27 Snapshots of *Pmm*2 $Tc_7Al_3B_4$ supercell (2×2×2) at ambient pressure at the end of 12 ps.

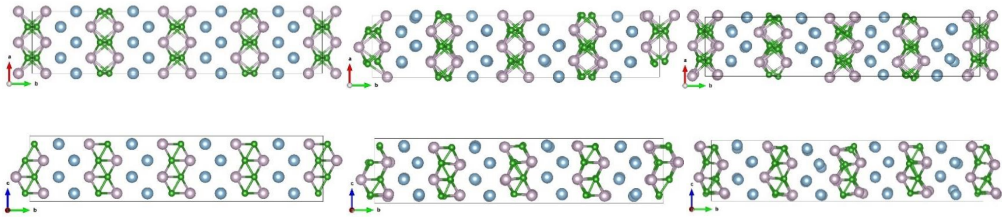

0K 600K 1000K

Fig. S28 Snapshots of *Cmcm* TcAlB supercell (2×2×2) at ambient pressure at the end of 12 ps.

S3.4 Electronic band structure and DOS

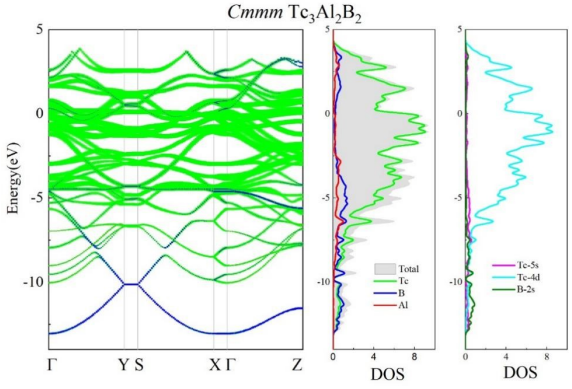

Fig. S29 Projected band structure and DOS of *Cmmm* $Tc_3Al_2B_2$

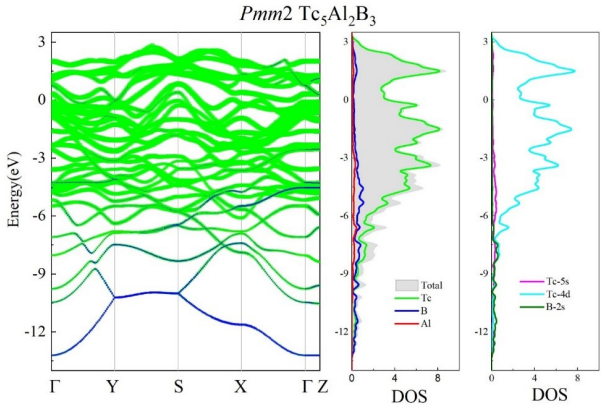

Fig. S30 Projected band structure and DOS of *Pmm2* $Tc_5Al_2B_3$

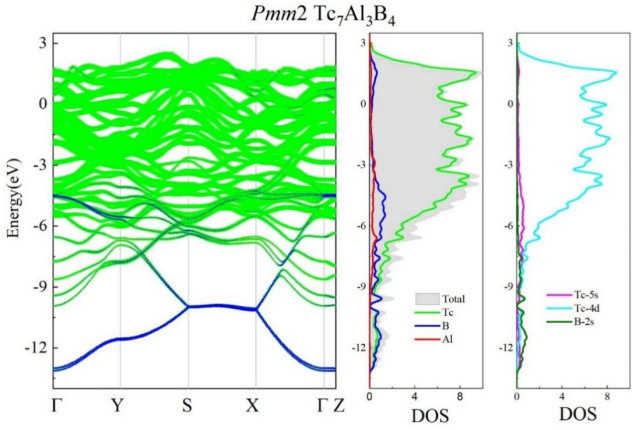

Fig. S31 Projected band structure and DOS of *Pmm2* $Tc_7Al_3B_4$

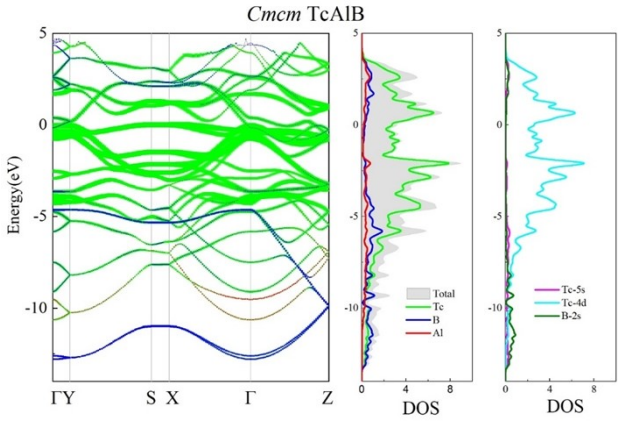

Fig. S32 Projected band structure and DOS of *Cmcm* TcAlB

S4 From bulk Tc-Al-B compounds to 2D Tc_2B_2 structure

S4.1 Force constants and ICOHP in bulk Tc-Al-B compounds

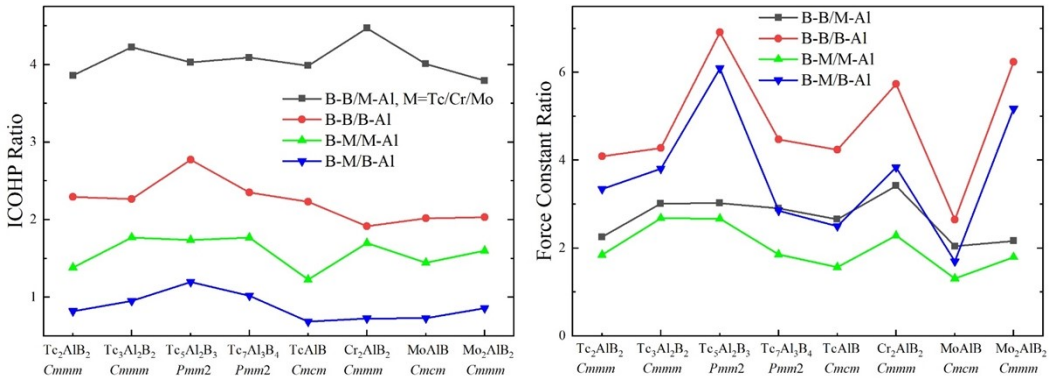

Fig. S33 ICOHP and force constant ratios: B-B/M-Al, B-B/B-Al, B-M/M-Al, and B-M/B-Al

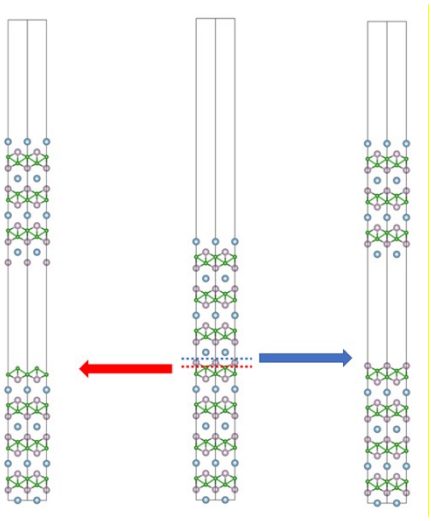

Fig. S34 Schematic diagram for the calculation of bonding energy at B/M (red) and M/Al (blue) interfaces in *Cmmm* Tc_2AlB_2.

S4.2 Dynamical stability

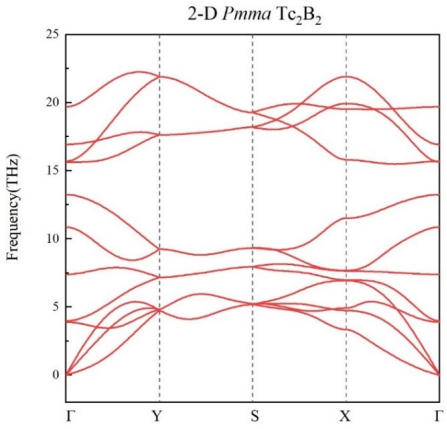

Fig. S35 Phonon dispersion curve of 2D Tc_2B_2 structures

S4.3 Thermal (kinetic) stability

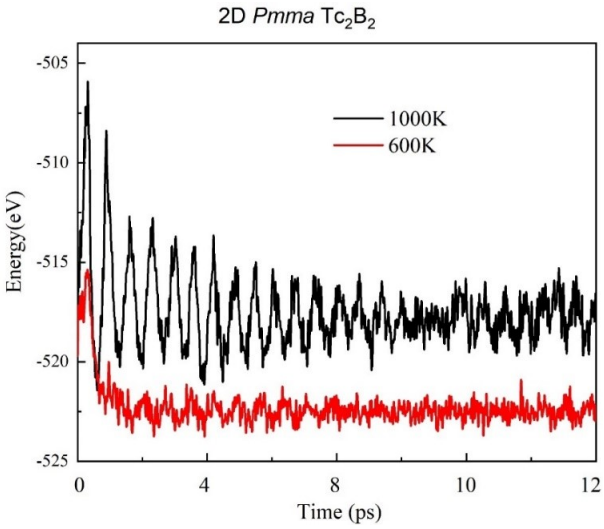

Fig. S36 Energy fluctuation of 2D *Pmma* Tc_2B_2 structure during the AIMD simulations at specific temperatures, T = 600K, 1000K.

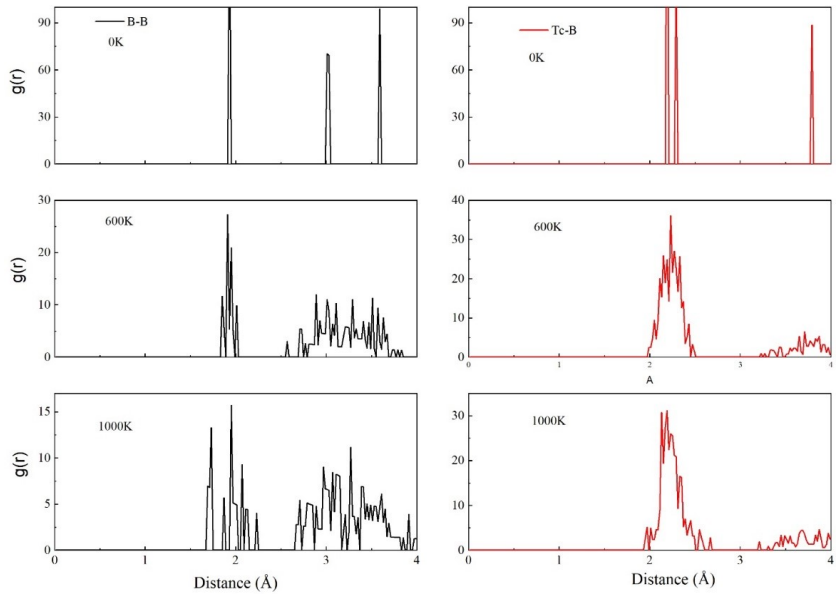

Fig. S37 Radial distribution functions (RDF) for the B-B, Tc-B contacts observed in 2D *Pmma* Tc_2B_2 structure during AIMD simulations at T = 0 K, 600 K, 1000 K.

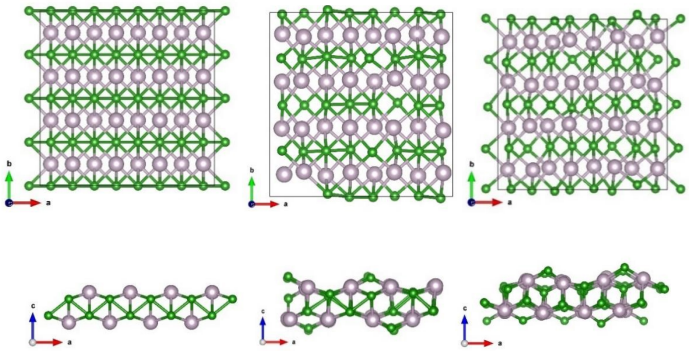

Fig. S38 Snapshots of 2D *Pmma* Tc_2B_2 supercell (4×4) at ambient pressure at the end of 12 ps, T=0K, 600K, 1000K.

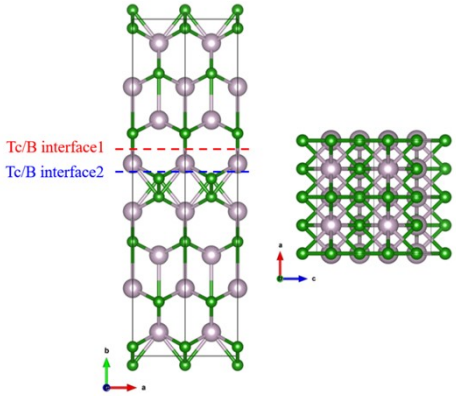

Fig. S39 Side and top view of bulk *Cmcm* TcB (2×1×2 supercell)

S5 Surface functionalization of 2D Tc_2B_2 structure

S5.1 Adsorption energy of ligands on 2D Tc_2B_2

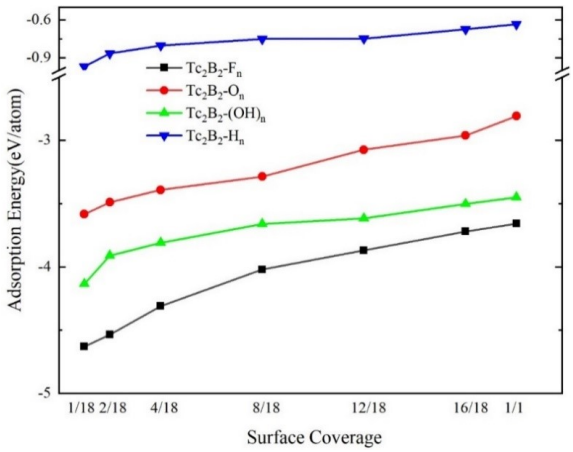

Fig. S40 Adsorption energy of functional groups -F, -O, -OH and -H on 2D Tc_2B_2 surface with the variation of surface coverage.

S5.2 ELF in surface functionalized 2D Tc_2B_2

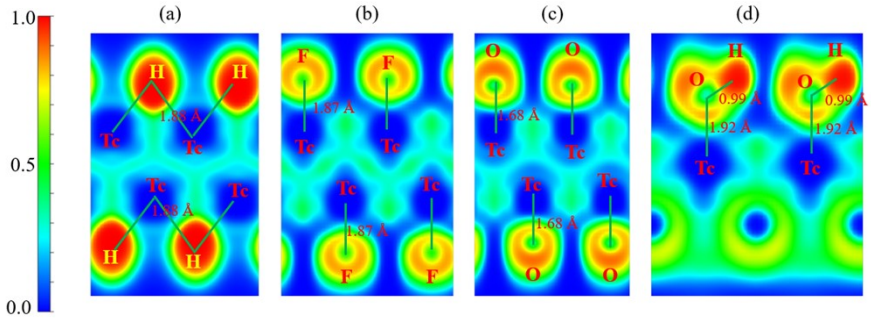

Fig. S41 Isosurface of ELF contours of H, F, O, OH functionalized 2D Tc_2B_2 structures in the full coverage.

S5.3 Dynamical stability

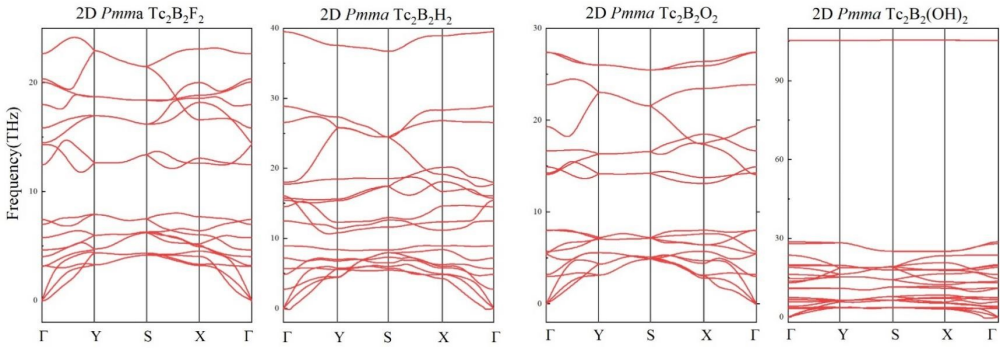

Fig. S42 Phonon dispersion curves of 2D *Pmma* Tc_2B_2 surface functionalized derivatives. Frequency range for $Tc_2B_2(OH)_2$ is much larger, owing to high frequency O-H vibrations.

S5.4Thermal (kinetic) stability

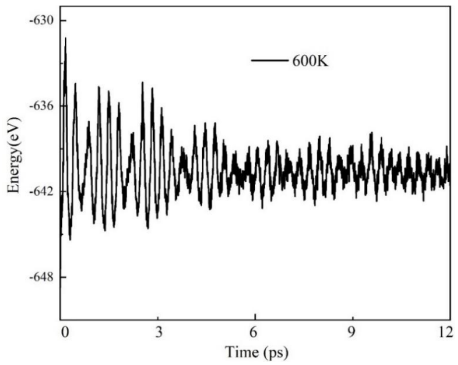

Fig. S43 Energy fluctuation of 2D *Pmma* $Tc_2B_2H_2$ during the AIMD simulations at specific temperatures, T = 600K. At 1000K, Tc-H bonds in 2D *Pmma* $Tc_2B_2H_2$ will break.

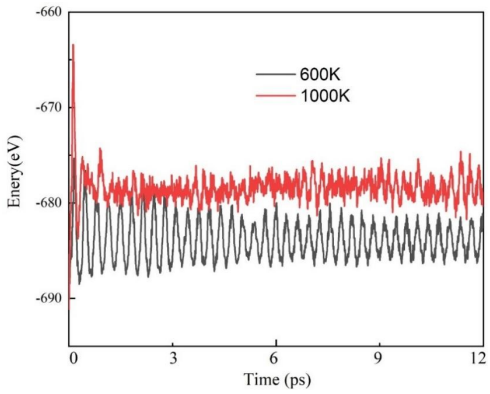

Fig. S44 Energy fluctuation of 2D *Pmma* $Tc_2B_2F_2$ during the AIMD simulations at specific temperatures, T = 600K, 1000K.

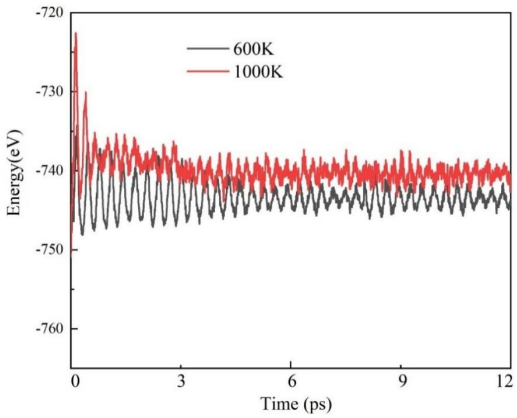

Fig. S45 Energy fluctuation of 2D *Pmma* $Tc_2B_2O_2$ during the AIMD simulations at specific temperatures, T = 600K, 1000K.

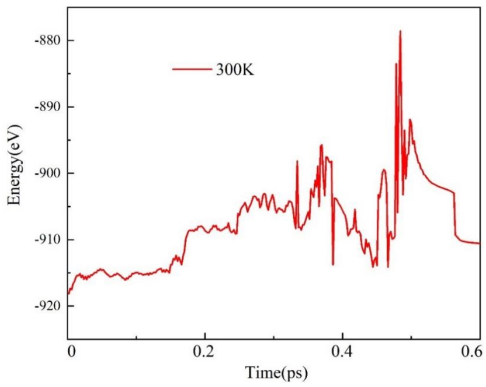

Fig. S46 Energy fluctuation of 2D $P2_1/m$ $Tc_2B_2(OH)_2$ during the AIMD simulations at specific temperatures, T = 300K. At the end of 0.6 ps, O-H bond breaks and then AIMD in VASP failed to continue.

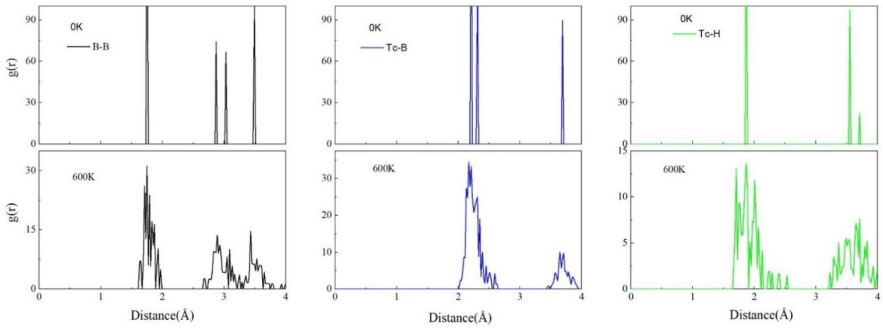

Fig. S47 Radial distribution functions (RDF) for the B-B, Tc-B, Tc-H contacts in 2D *Pmma* $Tc_2B_2H_2$ during AIMD simulations at T = 0 K, 600 K, 1000 K.

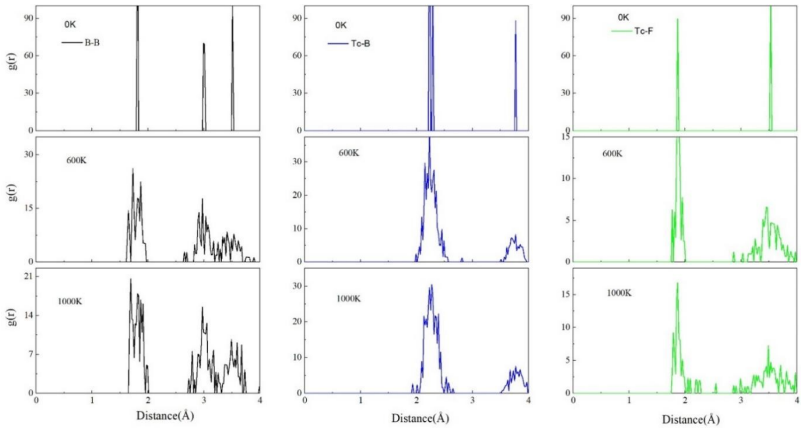

Fig. S48 Radial distribution functions (RDF) for the B-B, Tc-B, Tc-F contacts in 2D *Pmma* $Tc_2B_2F_2$ during AIMD simulations at T = 0 K, 600 K, 1000 K.

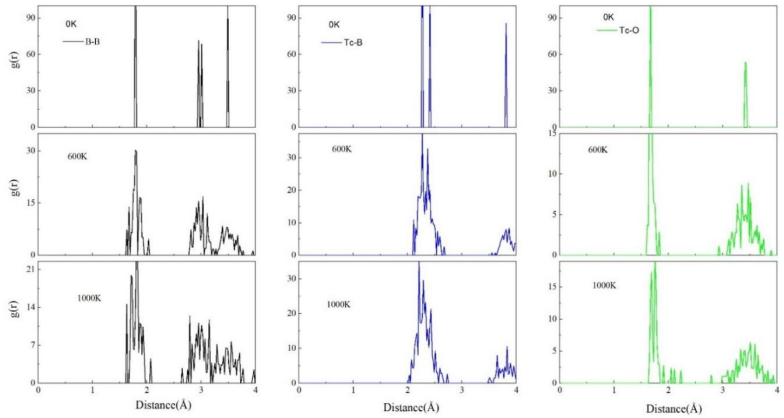

Fig. S49 Radial distribution functions (RDF) for the B-B, Tc-B, Tc-O contacts in 2D *Pmma* $Tc_2B_2O_2$ during AIMD simulations at T = 0 K, 600 K, 1000 K.

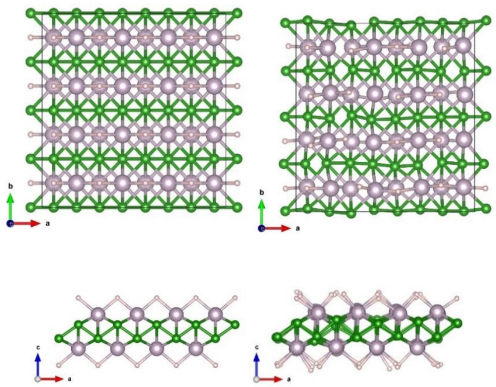

0K 600K

Fig. S50 Snapshots of 2D *Pmma* $Tc_2B_2H_2$ supercell (4×4) at ambient pressure at the end of 12 ps, T=0K, 600K.

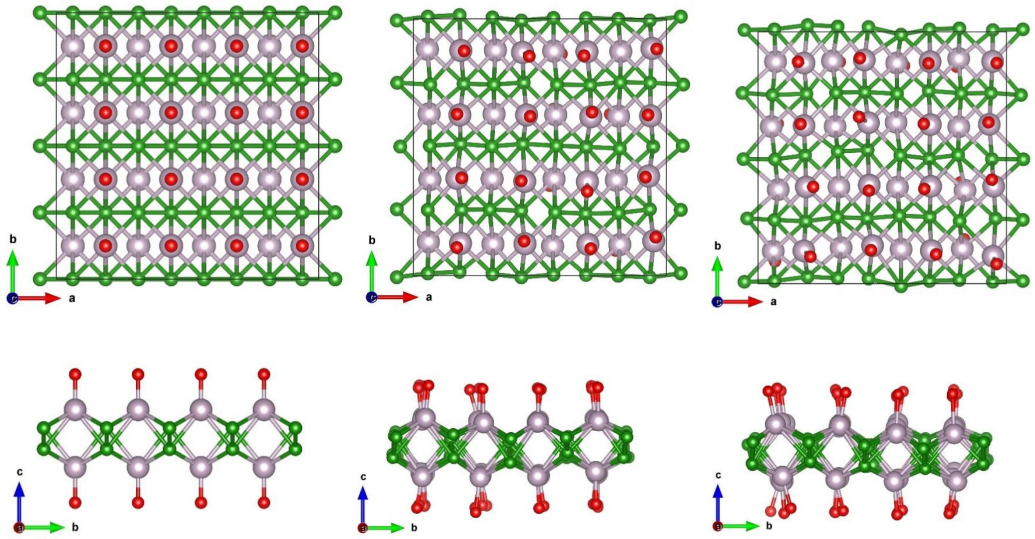

0K 600K 1000K

Fig. S51 Snapshots of 2D *Pmma* $Tc_2B_2O_2$ supercell (4×4) at ambient pressure at the end of 12 ps.

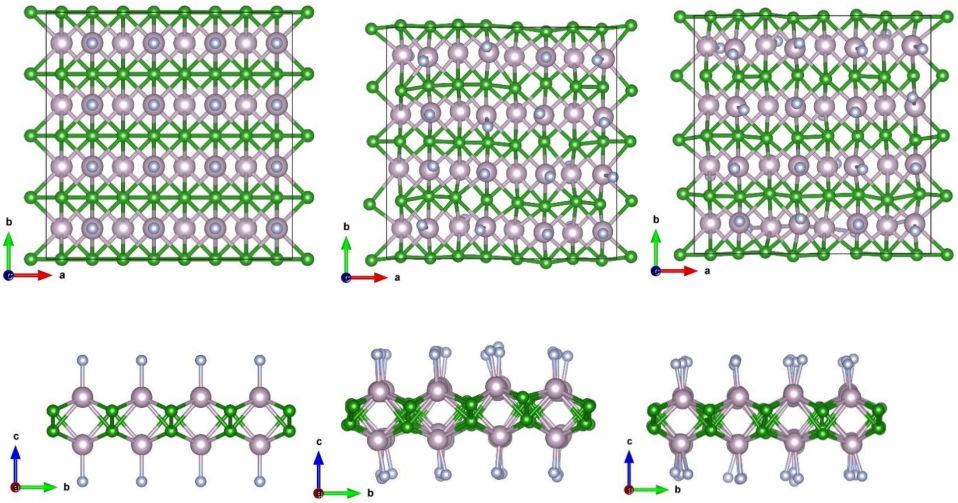

0K 600K 1000K

Fig. S52 Snapshots of 2D *Pmma* $Tc_2B_2F_2$ supercell (4×4) at ambient pressure at the end of 12 ps, T=0K, 600K, 1000K.

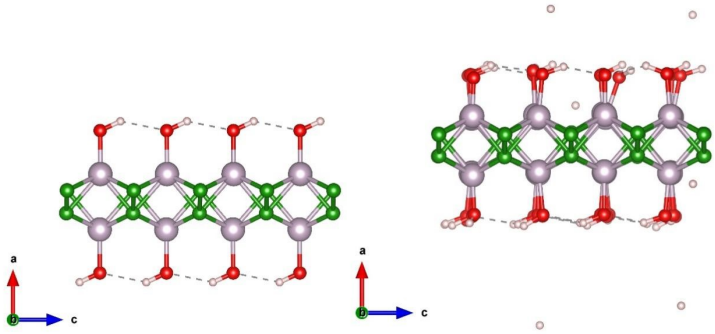

Fig. S53 Snapshots of 2D $P2_1/m$ $Tc_2B_2(OH)_2$ supercell (4×4) at ambient pressure at the end of 0.6 ps, T=0K, 300K.

S5.5 Electronic band structure and DOS

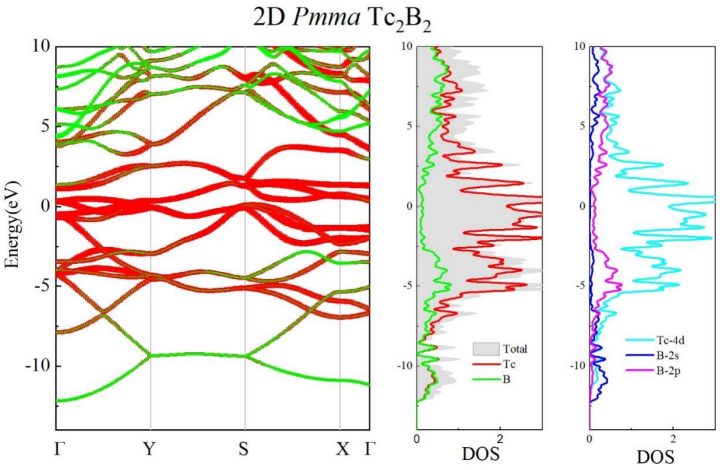

Fig. S54 Projected band structure and DOS of 2D *Pmma* Tc_2B_2

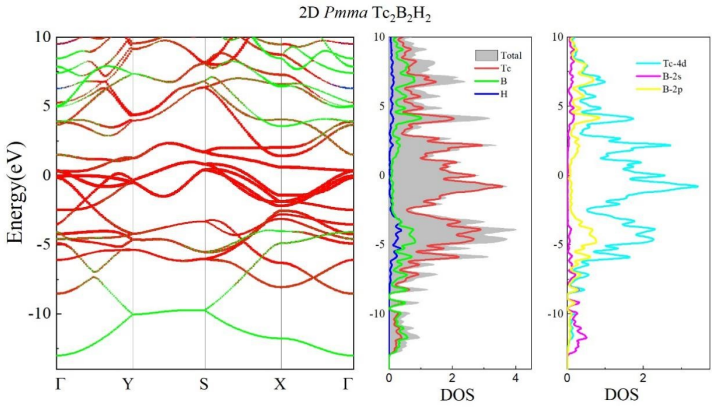

Fig. S55 Projected band structure and DOS of 2D *Pmma* $Tc_2B_2H_2$

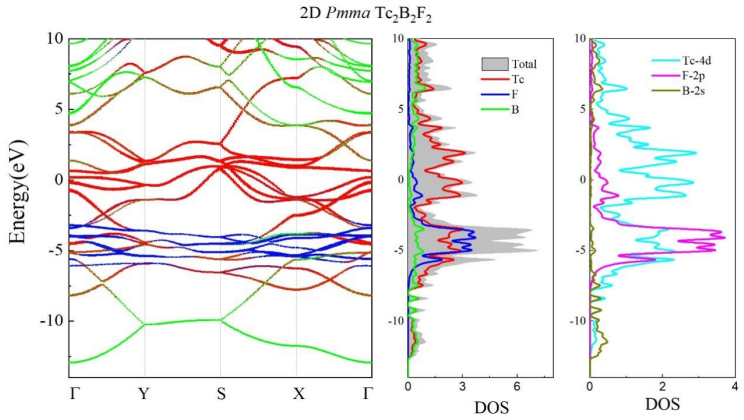

Fig. S56 Projected band structure and DOS of 2D *Pmma* $Tc_2B_2F_2$.

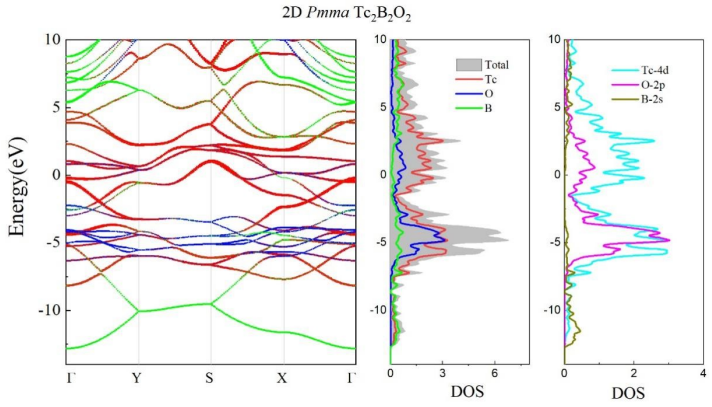

Fig. S57 Projected band structure and DOS of 2D *Pmma* $Tc_2B_2O_2$

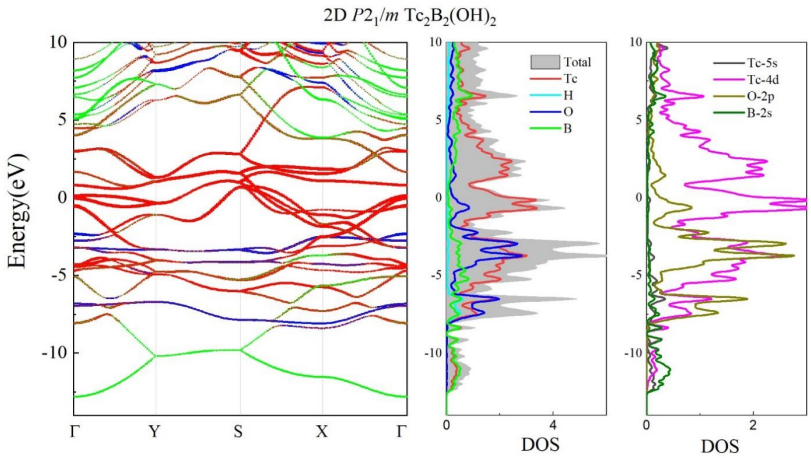

Fig. S58 Projected band structure and DOS of 2D $P2_1/m$ $Tc_2B_2(OH)_2$.

S6 Enthalpies, crystal parameters, bonding strength and mechanical properties

Table S1 Enthalpies of stable elementary (Tc, Al, B), binary (Tc_2Al, $TcAl_2$, $TcAl_3$, $TcAl_4$, Al_7B_{15}, Tc_3B, Tc_7B_3, TcB_2, TcB_3), ternary phases (Tc_2AlB_2) at ambient condition

bulk phase	Space group	Z	Enthalpy (eV/f.u.)	Formation enthalpy (eV/atom)	ZPE (eVf.u.)	Formation enthalpy (PBE+ZPE) (eV/atom)
Tc	$P6_3/mmc$ SG 194	2	-10.375	0.000	0.016	0.000
Al	*Fm*-3*m* SG 225	4	-3.750	0.000	0.131	0.000
B	*R*-3*m* SG 166	12	-6.705	0.000	0.037	0.000
Tc_2Al	*I*4/*mmm* SG 139	2	-25.691	-0.397	0.149	-0.370
$TcAl_2$	*Cmcm* SG 63	2	-19.177	-0.434	0.140	-0.417
$TcAl_3$	*C*2 SG 5	6	-23.303	-0.419	0.190	-0.403

$TcAl_4$	*Cm* SG 8	6	-27.137	-0.352	0.221	-0.341
$TcAl_{12}$	*Im*-3 SG 204	2	-57.451	-0.160	0.552	-0.152
Al_7B_{15}	*P*-1 SG 2	2	-127.963	-0.052	2.100	-0.057
Tc_3B	*Cmcm* SG 63	4	-38.885	-0.264	0.198	-0.263
Tc_7B_3	$P6_3mc$ SG 186	2	-95.825	-0.308	0.528	-0.306
TcB_2	$P6_3/mmc$ SG 194	2	-25.094	-0.436	0.264	-0.441
TcB_3	*P*-6*m*2 SG 187	1	-31.781	-0.323	0.369	-0.333
Tc_2AlB_2	*Cmmm* SG 65	2	-40.129	-0.444	0.352	-0.439

Table S2 Structural parameters of stable elementary (Tc, Al, B), binary (Tc_2Al, $TcAl_2$, $TcAl_3$, $TcAl_4$, Al_7B_{15}, Tc_3B, Tc_7B_3, TcB_2, TcB_3), ternary phases (Tc_2AlB_2) at ambient condition (distances in Å, angles in °)

bulk phase	Space group	Z	Lattice parameter (Å, °)	Atomic coordination
Tc	$P6_3/mmc$ SG 194	2	a=b=2.742, c=4.391 α=β=90.0, γ=120.0 *a=2.740, c=4.398[26]	2d (0.333 0.667 0.750)
Al	*Fm*-3*m* SG 225	4	a=b=c=4.036, α=β=γ=90.0 *a=b=c=4.046[27]	4a (0.000 0.000 0.000)
B	*R*-3*m* SG 166	12	a=b=c=5.049 α=β=γ=58.0	6h (0.010 0.010 0.654) 6h (0.221 0.221 0.630)

			a=b=c=5.050[28]	
Tc_2Al	*I*4/*mmm* SG 139	2	a=b=c=2.984, α=β=γ=90.0 *a=b=c=2.992[29]	Tc 4e (0.500 0.500 0.170) Al 2a (0.000 0.000 0.000)
$TcAl_2$	*Cmcm* SG 63	2	a=3.319, b=13.073, c=4.016, α=β=γ=90.0	Tc 4c (0.000 0.400 0.750) Al 4c (0.500 0.434 1.250) Al 4c (0.500 0.246 0.750)
$TcAl_3$	*C*2 SG 5	6	a=8.498, b=4.681, c=14.401 α=γ=90.0, β=141.9	Tc 4c (0.360 0.170 0.769) Tc 2b (0.000 0.672 0.500) Al 4c (0.334 0.828 0.999) Al 4c (0.160 0.172 0.503) Al 4c (0.519 0.671 0.263) Al 4c (0.834 0.672 0.255) Al 2a (0.500 0.339 0.000)
$TcAl_4$	*Cm* SG 8	6	a=5.201, b=17.618, c=5.161, α=γ=90.0, β=100.9 *a=5.1(1), b= 17.0(1), c=5.l (1), β=100(1)[29]	Tc 2a (0.488 0.500 0.054) Tc 4b (0.832 0.363 0.392) Al 4b (0.820 0.120 0.279) Al 4b (0.679 0.375 0.870) Al 4b (0.157 0.424 0.744) Al 4b (0.686 0.234 0.649) Al 4b (0.521 0.249 0.129) Al 2a (0.647 0.500 0.568) Al 2a (0.995 0.500 0.208)
$TcAl_{12}$	*Im*-3 SG 204	2	a=b=c=7.532, α=γ=β=90.0 *a=b=c=7.527[29]	Tc 2a (0.000 0.000 0.000) Al 24g (0.692 0.187 0.000)
Al_7B_{15}	*P*-1 SG 2	2	a=6.190, b=10.094, c=6.853, α=99.6, β=112.9, γ=96.5	B 2i (0.901 0.812 0.223) B 2i (0.900 0.589 0.778) B 2i (0.702 0.656 0.111) B 2i (0.700 0.545 0.889)

				B 2i (0.699 0.322 0.444) B 2i (0.499 0.611 0.221) B 2i (0.501 0.278 0.557) B 2i (0.302 0.121 0.446) B 2i (0.100 0.078 0.556) B 2i (0.899 0.145 0.888) B 2i (0.899 0.256 0.110) B 2i (0.700 0.989 0.778) B 2i (0.703 0.210 0.224) B 2i (0.500 0.055 0.111) B 2i (0.101 0.523 0.444) Al 2i (0.500 0.831 0.165) Al 2i (0.304 0.564 0.823) Al 2i (0.106 0.630 0.172) Al 2i (0.114 0.307 0.502) Al 2i (0.703 0.102 0.501) Al 2i (0.308 0.243 0.180) Al 2i (0.099 0.967 0.833)
Tc_3B	*Cmcm* SG 63	4	a=2.914, b=9.227, c=7.212, α=γ=β=90.0 *a=2.891, b=9.161, c=7.246[26]	Tc 8f (0.000 0.865 0.439) Tc 4c (0.000 0.575 0.250) B 4c (0.500 0.756 0.250)
Tc_7B_3	$P6_3mc$ SG 186	2	a=b=7.482, c=4.849 α=β=90.0, γ=120.0 *a=7.417, c=4.777[26]	Tc 6c (0.454 0.909 0.048) Tc 6c (0.876 0.753 0.255) Tc 2b (0.667 0.333 0.086) B 6c (0.621 0.810 0.340)
TcB_2	$P6_3/mmc$ SG 194	2	a=b=2.897, c=7.461 α=β=90.0, γ=120.0 *a=2.892, c=7.452[26]	Tc 2d (0.667 0.333 0.250) B 4f (0.333 0.667 0.048)

TcB_3	*P*-6*m*2 SG 187	1	a=b=2.907, c=4.572 α=β=90.0, γ=120.0 *a=2.871, c=4.535[30]	Tc 1b (0.000 0.000 0.500) B 1a (0.000 0.000 0.000) B 2h (0.333 0.667 0.819)
Tc_2AlB_2	*Cmmm* SG 65	2	a=11.574, b=3.040, c=3.014, α=β=γ=90.0,	Tc 4h (0.139 0.500 0.500) Al 2a (0.000 0.000 0.000) B 4g (0.293 0.500 0.00)

* indicates the experimental and theoretical lattice parameters in the literatures.

Table S3 Elastic constants C_{ij} (GPa) in bulk *P*-1 Al_7B_{15}, *Cmcm* $TcAl_2$, and *C*2 $TcAl_3$.

	Al_7B_{15}	$TcAl_2$	$TcAl_3$	Tc_2AlB_2
Space group	*P*-1 SG 2	*Cmcm* SG 63	*C*2 SG 5	*Cmmm* SG 65
C_{11}	347.505	266.762	246.841	330.874
C_{12}	108.192	97.076	82.672	198.923
C_{13}	124.726	130.567	87.023	180.332
C_{14}	-45.921	0.000	0.000	0.000
C_{15}	-90.591	0.000	-11.386	0.000
C_{16}	81.755	0.000	0.000	0.000
C_{22}	340.988	280.365	248.956	481.013
C_{23}	118.666	77.341	55.4778	139.709
C_{24}	80.172	0.000	0.000	0.000
C_{25}	61.550	0.000	8.903	0.000
C_{26}	64.072	0.000	0.000	0.000
C_{33}	315.506	306.980	287.613	515.195
C_{34}	58.405	0.000	0.000	0.000
C_{35}	-56.156	0.000	-12.526	0.000
C_{36}	-67.252	0.000	0.000	0.000
C_{44}	218.693	92.966	84.891	165.376
C_{45}	-53.194	0.000	0.000	0.000

C_{46}	35.074	0.000	5.702	0.000
C_{55}	208.524	148.906	125.990	130.830
C_{56}	-20.660	0.000	0.000	0.000
C_{66}	207.460	121.546	116.165	120.332

Table S4 Enthalpies of metastable ternary Tc-Al-B compounds at ambient condition.

bulk phase	Space group	Z	Enthalpy (eV/f.u.)	Formation enthalpy (eV/atom)	ZPE (eV/f.u.)	Formation enthalpy (PBE+ZPE) (eV/atom)
$Tc_3Al_2B_2$	*Cmcm* SG65	2	-54.927	-0.413	0.414	-0.409
$Tc_5Al_2B_3$	*Pmm*2 SG25	1	-83.263	0.-377	0.602	-0372
$Tc_7Al_3B_4$	*Pmm*2 SG25	1	-115.621	-0.352	0.774	-0.350
TcAlB	*Cmcm* SG63	4	-21.884	-0.351	0.187	-0.350

Table S5 Structural parameters of metastable ternary Tc-Al-B compounds at ambient condition (distances in Å, angles in °)

bulk phase	Space group	Z	Lattice parameter (Å, °)	Atomic coordination
$Tc_3Al_2B_2$	*Cmmm* SG 65	2	a=3.049, b=17.452, c=3.064 α=β=γ=90.0	Tc 2a (0.000 0.0000 0.000) Tc 2j (0.000 0.181 0.000) B 4j (0.000 0.279 0.500) Al 4j (0.000 0.418 0.5000)
$Tc_5Al_2B_3$	*Pmm*2 SG 25	1	a=2.995, b=2.995, c=13.013	Tc 1b (0.000 0.500 0.592) Tc 1b (0.000 0.500 0.342)

			α=β=γ=90.0	Tc 1d (0.500 0.500 0.146) Tc 1d (0.500 0.500 0.893) Tc 1c (0.500 0.000 0.709) Al 1a (0.000 0.000 0.016) Al 1c (0.500 0.000 0.473) B 1c (0.500 0.000 0.284) B 1a (0.000 0.000 0.205) B 1a (0.000 0.000 0.836)
$Tc_7Al_3B_4$	*Pmm*2 SG 25	1	a=3.021, b=3.045, c=17.808 α=β=γ=90.0	Tc 1a (0.000 0.000 0.000) Tc 1a (0.000 0.000 0.822) Tc 1a (0.000 0.000 0.178) Tc 1c (0.500 0.000 0.497) Tc 1c (0.500 0.000 0.318) Tc 1c (0.500 0.000 0.687) Tc 1b (0.000 0.500 0.582) Al 1b (0.000 0.500 0.412) Al 1d (0.500 0.500 0.082) Al 1d (0.500 0.500 0.919) B 1b (0.000 0.500 0.723) B 1b (0.000 0.500 0.276) B 1d (0.500 0.500 0.219) B 1d (0.500 0.500 0.783)
TcAlB	*Cmcm* SG63	4	a=3.024, b=14.110, c=3.163 α=β=γ=90.0	Tc 4c (0.500 0.594 0.250) B 4c (0.500 0.969 0.250) Al 4c (0.000 0.697 0.750)

Table S6 Elastic constants C_{ij} (GPa) in ternary Tc-Al-B phases

	$Tc_3Al_2B_2$	$Tc_5Al_2B_3$	$Tc_7Al_3B_4$	TcAlB
Space group	*Pmm*2 SG 25	*Pmm*2 SG 25	*Pmm*2 SG 25	*Cmcm* SG63

C_{11}	372.727	487.803	402.259	385.476
C_{12}	188.830	150.791	164.062	161.954
C_{13}	153.050	179.973	210.762	146.202
C_{22}	304.599	447.570	377.452	290.309
C_{23}	185.491	173.894	196.925	174.278
C_{33}	339.287	350.460	293.797	359.323
C_{44}	102.287	128.061	119.891	113.408
C_{55}	139.925	144.018	117.310	143.621
C_{66}	123.295	152.846	158.359	169.029

Table S7 The bonding strength (Mulliken population, force constants and ICOHP) between bonds within the M_2B_2 sublattice (B-B and B-M bonds) and bonds at the interface of M_2B_2 sublattice and Al layer (B-Al and M-Al bonds) in selected $M_xAl_yB_z$ compounds, M=Tc/Cr/Mo.

Bonds	Bonding Strength	Cr_2AlB_2 *Cmmm*	MoAlB *Cmcm*	Mo_2AlB_2 *Cmmm*	Tc_2AlB_2 *Cmmm*	$Tc_3Al_2B_2$ *Cmmm*	$Tc_5Al_2B_3$ *Pmm*2	$Tc_7Al_3B_4$ *Pmm*2	TcAlB *Cmcm*
B-B	Mulliken Population	1.33	1.38	1.29	1.28	1.53	1.25	1.24	1.36
	-ICOHP	4.56	5.41	5.12	5.75	5.49	5.68	5.48	6.02
	Force Constant	6.94	5.14	4.74	5.23	3.98	4.63	4.56	5.55
B-Tc	Mulliken Population	0.78	0.66	0.72	0.79	0.85	0.87	0.85	0.63
	-ICOHP	1.73	1.95	2.16	2.06	2.3	2.45	2.37	1.85
	Force Constant	4.64	3.29	3.93	4.28	3.54	4.08	2.91	3.27
Tc-Al	Mulliken Population	0.51	0.73	0.56	0.5	0.36	0.48	0.49	0.72
	-ICOHP	1.02	1.35	1.35	1.49	1.3	1.41	1.34	1.51

	Force Constant	2.03	2.52	2.19	2.32	1.32	1.53	1.57	2.09
B-Al	Mulliken Population	0.12	0.16	0.13	0.09	0.09	0.05	0.07	0.12
	-ICOHP	2.38	2.68	2.52	2.51	2.42	2.05	2.33	2.7
	Force Constant	1.21	1.94	0.76	1.28	0.93	0.67	1.02	1.31

Table S8 Structural parameters of 2D Tc_2B_2 (distances in Å, angles in °). The thickness of 2D Tc_2B_2 is listed.

2D phase	Space group	Z	Lattice parameter (Å, °)	Atomic coordination	Thickness (Å)
Tc_2B_2	*Pmma* SG 51	2	a=3.014, b=3.022, c=17.573 α=β=γ=90.0	Tc 2f (0.250 0.500 0.437) B 2e (0.250 0.000 0.535)	2.22

Table S9 Elastic constants C_{11}, C_{12}, C_{22}, C_{66} (N/m) in 2D Tc_2B_2

2D phase	Space group	C_{11}	C_{12}	C_{22}	C_{66}
Tc_2B_2	*Pmma* SG 51	194.062	102.594	232.371	71.377

Table S10 Structural parameters of surface functionalized derivatives of 2D Tc_2B_2 (distances in Å, angles in °). The thickness of Tc_2B_2 slab in 2D $Tc_2B_2X_2$ (X=H, F, O, OH) is listed.

2D phase	Space group	Z	Lattice parameter (Å, °)	Atomic coordination	Thickness (Å)
$Tc_2B_2H_2$	*Pmma* SG 51	2	a=2.869, b=2.022, c=17.846 α=β=γ=90.0	Tc 2f (0.750 0.500 0.569) B 2e (0.750 0.000 0.471) H 2f (0.250 0.500	2.50

				0.638)	
$Tc_2B_2F_2$	*Pmma* SG 51	2	a=2.995, b=3.004, c=17.537 α=β=γ=90.0	Tc 2f (0.250 0.500 0.569) B 2e (0.250 0.000 0.471) F 2f (0.250 0.500 0.675)	2.42
$Tc_2B_2O_2$	*Pmma* SG 51	2	a=2.958, b=3.002, c=17.586 α=β=γ=90.0	Tc 2f (0.250 0.500 0.578) B 2e (0.250 0.000 0.471) O 2f (0.250 0.500 0.673)	2.74
$Tc_2B_2(OH)_2$	$P2_1/m$ SG 11	2	a=23.028, b=3.026, c=2.952 α=γ=90.0, β=91.0	Tc 2e (0.553 0.750 0.513) B 2e (0.478 0.750 0.991) O 2e (0.637 0.750 0.522) H 2e (0.654 0.750 0.828)	2.45

Table S11 Elastic constants C_{11}, C_{12}, C_{22}, C_{66} (N/m) in 2D Tc_2B_2 and corresponding surface functionalized derivatives.

2D phase	Space group	C_{11}	C_{12}	C_{22}	C_{66}
$Tc_2B_2H_2$	*Pmma* SG 51	328.681	58.651	256.425	68.878
$Tc_2B_2F_2$	*Pmma* SG 51	253.473	58.826	240.197	54.260
$Tc_2B_2O_2$	*Pmma* SG 51	259.800	47.669	272.255	59.042
$Tc_2B_2(OH)_2$	$P2_1/m$ SG 11	234.502	60.241	259.949	57.925

S7 Reference

1. A. R. Oganov, A. O. Lyakhov and M. Valle, *Acc. Chem. Res.*, 2011, **44**, 227-237.
2. A. R. Oganov and C. W. Glass, *J. Chem. Phys.*, 2006, **124**, 201-419.
3. A. O. Lyakhov, A. R. Oganov, H. T. Stokes and Q. Zhu, *Comput. Phys. Commun.*, 2013, **184**, 1172-1182.
4. G. G. Kresse and J. J. Furthmüller, *Phys. Rev. B Condens. Matter*, 1996, **54**, 11169.
5. E. P. Blöchl, *Phys. Rev. B*, 1994, **50**, 17953-17979.
6. J. P. Perdew, K. Burke and M. Ernzerhof, *Phys. Rev. Lett.*, 1998, **80**, 891-891.
7. J. P. Perdew, K. Burke and M. Ernzerhof, *Phys. Rev. Lett.*, 1998, 77, 3865-3868.
8. S. Nos'E, *J. Chem. Phys.*, 1984, **81**, 511-511.
9. A. Togo, F. Oba and I. Tanaka, *Phys. Rev. B*, 2008, **78**, 134106.
10. M. Khazaei, A. Ranjbar, K. Esfarjani, D. Bogdanovski, R. Dronskowski and S. Yunoki, *Phys. Chem. Chem. Phys.*, 2018, **20**, 8579-8592.
11. A. Foreman and W. Lomer, *Proc. Phys. Soc. Section B*, 1957, **70**, 1143.
12. Y. Liu, K. T. E. Chua, T. C. Sum and C. K. Gan, *Phys. Chem. Chem. Phys.*, 2014, **16**, 345-350.
13. M. Segall, C. Pickard, R. Shah and M. Payne, *Mol. Phys.*, 1996, 89, 571-577.
14. M. Segall, R. Shah, C. J. Pickard and M. Payne, *Phys. Rev. B*, 1996, 54, 16317.
15. D. Sanchez-Portal, E. Artacho and J. M. Soler, *Solid State Commun.*, 1995, **95**, 685-690.
16. R. S. Mulliken, *J. Chem. Phys.*, 1955, **23**, 1833-1840.
17. M. Born and K. Huang, *Dynamical theory of crystal lattices*, *Clarendon press*, 1954.
18. F. Mouhat and F.-X. Coudert, *Phys. Rev. B*, 2014, **90**, 224104.
19. R. Cowley, *Phys. Rev. B*, 1976, **13**, 4877.
20. Y. Le Page and P. Saxe, *Phys. Rev. B*, 2002, **65**, 104104.
21. C. Jasiukiewicz, T. Paszkiewicz and S. Wolski, *Phys. Status Solidi B*, 2008, **245**, 557-561.
22. R. C. Andrew, R. E. Mapasha, A. M. Ukpong and N. Chetty, *Phys. Rev. B*, 2012, **85**, 125428.
23. Z. Guo, J. Zhou and Z. Sun, *J. Mater. Chem. A*, 2017, **5**, 23530-23535.
24. J. H. Jung, C.-H. Park and J. Ihm, *Nano Lett.*, 2018, **18**, 2759-2765.

25. M. Khazaei, M. Arai, T. Sasaki, C. Y. Chung, N. S. Venkataramanan, M. Estili, Y. Sakka and Y. Kawazoe, *Adv. Funct. Mater.*, 2013, **23**, 2185-2192.
26. W. Trzebiatowski and J. Rudzinski, *J. Less-Common Metals*, 1964, **6**, 244-245
27. W. P. Davey, *Phys. Rev.*, 1925, **25**, 753.
28. A. Jain, S. P. Ong, G. Hautier, W. Chen, W. D. Richards, S. Dacek, S. Cholia, D. Gunter, D. Skinner and G. Ceder, *APL Mater.*, 2013, **1**, 011002.
29. L. D'Alte Da Veiga and L. Walford, *Philos. Mag.*, 1963, **8**, 349-349.
30. C. Ying, T. Liu, L. Lin, E. Zhao and Q. Hou, *Comput. Mater. Sci.*, 2018, ***144***, 154-160.